Nanoparticles for solid rocket propulsion

2006 J. Phys.: Condens. Matter 18 S1991

(http://iopscience.iop.org/0953-8984/18/33/S15)

INSTITUTE OF PHYSICS PUBLISHING JOURNAL OF PHYSICS: CONDENSED MATTER

J. Phys.: Condens. Matter **18** (2006) S1991–S2005 doi:10.1088/0953-8984/18/33/S15

Nanoparticles for solid rocket propulsion

L Galfetti[1], L T De Luca[1], F Severini[1], L Meda[2], G Marra[2], M Marchetti[3], M Regi[3] and S Bellucci[4]

[1] Politecnico di Milano, SPLab, Milano, Italy
[2] Polimeri Europa, Istituto G Donegani, Novara, Italy
[3] Università di Roma 'La Sapienza', Dipartimento di Ingegneria Aerospaziale ed Astronautica, Roma, Italy
[4] INFN, Laboratori Nazionali di Frascati, Frascati, Italy

Received 21 April 2006, in final form 12 July 2006
Published 4 August 2006
Online at stacks.iop.org/JPhysCM/18/S1991

Abstract

The characterization of several differently sized aluminium powders, by BET (specific surface), EM (electron microscopy), XRD (x-ray diffraction), and XPS (x-ray photoelectron spectroscopy), was performed in order to evaluate their application in solid rocket propellant compositions. These aluminium powders were used in manufacturing several laboratory composite solid rocket propellants, based on ammonium perchlorate (AP) as oxidizer and hydroxil-terminated polybutadiene (HTPB) as binder. The reference formulation was an AP/HTPB/Al composition with 68/17/15% mass fractions respectively. The ballistic characterization of the propellants, in terms of steady burning rates, shows better performance for propellant compositions employing nano-aluminium when compared to micro-aluminium. Results obtained in the pressure range 1–70 bar show that by increasing the nano-Al mass fraction or decreasing the nano-Al size, larger steady burning rates are measured with essentially the same pressure sensitivity.

(Some figures in this article are in colour only in the electronic version)

Nomenclature

a	multiplicative factor in the Vieille steady burning rate law (mm s^{-1})
n	steady burning rate pressure sensitivity ((mm s^{-1})/(bar^n))
p	pressure (bar)
r_b	steady burning rate (mm s^{-1})
ρ	density (g cm^{-3})
BET	specific surface area measurement
EEW	electrical explosion of wires
SEM	scanning electron microscopy
TEM	transmission electron microscopy
XPS	x-ray photoelectron spectroscopy
XRD	x-ray diffraction

Table 1. Summary of micro and nano-Al powders investigated.

	Al powder notation	Production technique	Coating	Size (μm)	Ageing
Type 01	Al_01a	EEW	Uncoated	0.10	2002
	Al_02a				2003
Type 02	Al_02b	EEW	Uncoated	0.17	2002
	Al_02c				1999
	Al_03a			0.2	—
	Al_03b	Mechanical	Uncoated	0.4	—
Type 03	Al_03c			0.8	—
	Al_03d			2.5	—
Type 04	Al_04a	Plasma	Coated	0.20	—
	Al_04b	condensation		0.28	—
Type 05	Al_05	Mechanical	Uncoated	30 (spherical)	—
Type 06	Al_06	Mechanical	Uncoated	50 (flakes)	—

1. Introduction

A well-known way to increase the reactivity of powders is to decrease their particle size. Significant increases in propellant burning rates, shorter ignition delays and shorter agglomerates burning times were recently obtained for composite solid propellant formulations containing ultra-fine energetic particles, particularly Al nanoparticles [1–5]. Nanoparticles can enhance the linear burning rate of aluminized solid propellants by 100% or even more, but poor mechanical properties of the propellant and a higher content of condensed Al_2O_3 in the combustion residues, which is responsible for the specific impulse reduction, at present restrict the use of nanosized Al propellants and suggest further investigations. This is the reason for the extensive international research activity distributed in several laboratories [6–11].

A research program was planned to investigate properties, structure, composition of conventional sized Al powders and nanosized Al powders (from different suppliers, produced with different techniques, coated and uncoated) and to test the ballistic properties of AP/HTPB/Al composite propellants manufactured using these powders. Different series of aluminium powders have been analysed and their characterization properties compared. They have different particle size and morphology due to different preparation procedures. A comprehensive summary is presented in table 1; both nanometric (or ultra-fine) and micrometric (spheres or flakes) size ranges were investigated.

The aluminium nanopowders used in this experimental investigation are naturally protected by a thin layer of aluminium oxides which makes their handling possible. This protective layer preserves the metal from additional oxidation but the powder may be easily attacked by water, basic and acid solutions, with hydrogen development in the environment.

The aluminium powder Al_05 is a powder (spheres of 30 μm) used in industrial propellants, while the powder Al_06 is a cheap commercial powder (irregular flakes of 50 μm characteristic size) used for paints.

2. Experimental techniques for powder characterization

Different experimental techniques (BET, EM, XPS, XRD) were used to characterize the powders of table 1.

The measurement of the specific surface area was computed from the nitrogen adsorption isotherm obtained by static volumetric measurement at liquid nitrogen boiling temperature (77 K). Samples were outgassed at 100 °C for at least 4 h at absolute pressure less than 10^{-3} Torr. All measurements were carried out on a completely automated instrument (ASAP 2010 from Micromeritics®), leading to the final value of the specific surface areas expressed in $m^2\ g^{-1}$ (square metres per gram of sample).

Electron microscopy was used to study the shape, size, morphology and defects of powders. The results presented in this paper were obtained with an *SEM* microscope (Cambridge Stereoscan 360, maximum accelerating voltage 40 kV) with an ultimate resolving power of 3.5 nm.

XPS was used, in conjunction with 4 keV Ar^+ (Ar ion) sputtering, to obtain chemical depth profiles, to discover details about the surface passivation layers. In combination with ion etching, XPS line intensities allow an investigation of atomic composition in the subsurface region, up to depths of the order of hundreds of nanometres, and quantify the concentrations of main constitutive elements. Also possible contaminations, at a concentration level higher than 0.1 at.%, can be detected by this technique. The quantitative analysis allows one to know the atomic fraction of chemical elements, hydrogen excluded, so that the stoichiometric ratio and a chemical composition can be evaluated. XPS peak decomposition was carried out by considering the peaks to be 100% Gaussian, with binding energy (Al_{met}) 73.0 eV and with binding energy (Al_{ox}) = 74.5 eV.

The spectrometer is a PHI-model5500, with monochromatized aluminium source for x-ray production. Spectra were taken at 300 W and the sputtering rate has been estimated to be 5.5 nm min^{-1}.

XRD spectra were obtained to investigate the crystalline phases and their relative quantity. Previously, a qualitative analysis had been carried out by means of the standard powder method. In addition, a full-profile fitting procedure, based on the Rietveld method, allowed us to perform very accurate quantitative analysis and to get structural refinements of each identified phase. The code used was GSAS (generalized structure analysis system). We did not use any relative intensity ratios (RIR) method. XRD spectra were collected step-wise using Cu Kα radiation ($\lambda = 1.5416$ Å) on a computer controlled Philips X'Pert PRO $\theta/2\theta$ diffractometer, equipped with a secondary curved pyrolytic graphite monochromator, in the 5°–125° 2θ angular range, with 0.02° steps and 15 s counting time.

3. Experimental results

3.1. Specific surface area measurement (BET)

The specific surface area of only sub-micrometric Al particles was measured because the technique does not work for powders having larger particles (Al_05 and Al_06). Table 2 summarizes the results, which show the inverse relationship of powder nominal size with specific surface.

Experimental adsorption isotherms for the measured samples show that the trend of the powders Al_01a and Al_02c are typical of mesoporous materials with multilayer adsorption, while the powders Al_03a, Al_03b, and Al_03c are typical of non-porous materials with monolayer adsorption (Langmuir type). The reason for the difference from the two families has to be related to the powder production technique: EEW leaves mesocavities in particle aggregates, while mechanical milling leaves separated particles.

3.2. Scanning electron microscopy analysis (SEM)

The SEM micrographs show that, at a large scale (200×), powder Al_01a presents different types of irregular agglomerates of characteristic size up to 90 μm (figure 1(a)), but at higher

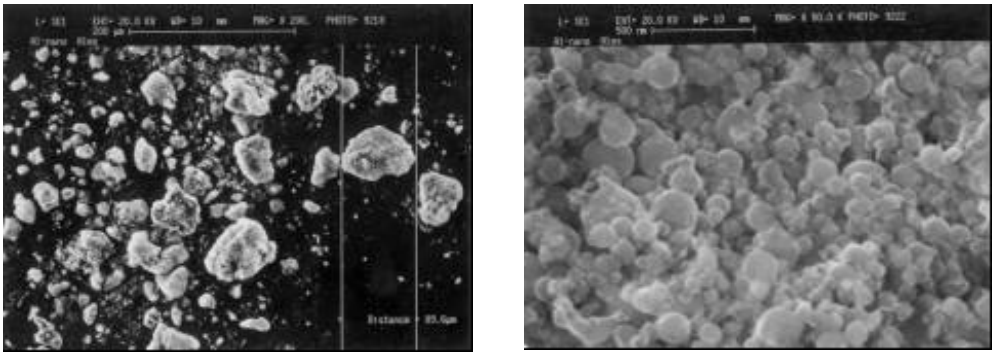

(a) (b)

Figure 1. SEM micrographs of powder Al_01a at different magnifications: (a) 200×; (b) 50 k×.

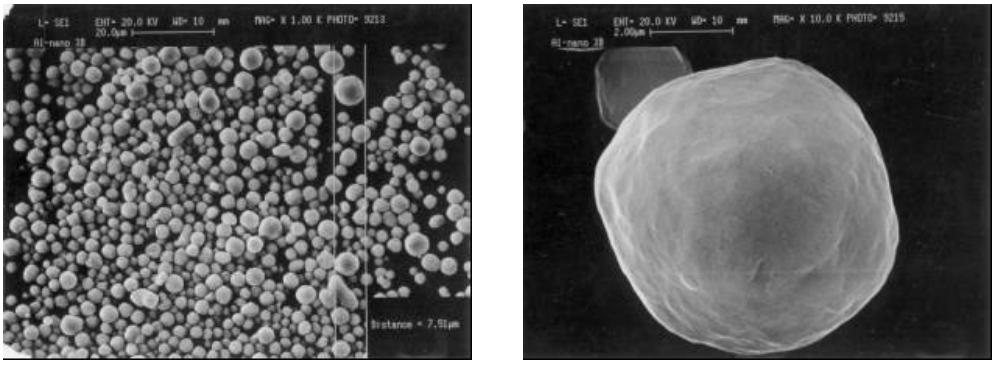

(a) (b)

Figure 2. SEM micrographs of powder Al_03d at different magnifications: (a) 1 k×; (b) 20 k×.

Table 2. Results of specific surfaces measured with BET technique.

Al powder notation	Nominal size (μm)	Specific surface ($m^2\ g^{-1}$)
Al_01a	0.10	15.6 ± 0.1
Al_02c	0.17	13.2
Al_03a	0.20	2.0
Al_03b	0.40	1.5
Al_03c	0.80	0.9
Al_03d	2.5	0.7
Al_05	30	<1
Al_06	50	(sensitivity threshold)

magnification (50 k×) it can be observed that they are formed by primary spherical particles, whose diameter is between 50 and 250 nm (figure 1(b)).

Sample Al_03-d is characterized by a completely spherical morphology of monodispersed particles at the largest scale (1 k×), whose range lies from 1 to 7 μm (figure 2(a)). Moreover, at higher magnification (10–20 k×) the absence of a nanometric structure inside the spherical particles can be clearly detected (figure 2(b)).

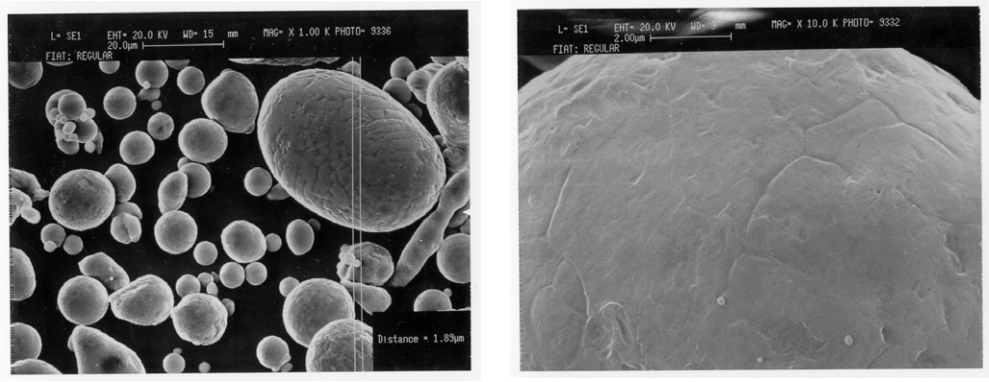

(a) (b)

Figure 3. SEM micrographs of powder Al_05 at different magnifications: (a) 1 k×; (b) 10 k×.

Similar results are obtained for sample Al_05: a more dispersed particle granulometry is observed at the smaller scale (1 k×, figure 3(a)); the shape is not as spherical as before and larger particles can be observed (from 1 to 70 μm). At higher magnification (10 k×) a compact morphology is visible with surface tracks and roughness (figure 3(b)).

3.3. X-ray photoelectron spectroscopy analysis (XPS)

By considering the whole aluminium peak after each sputtering cycle, the peak can be decomposed into metallic-Al and oxidized-Al components and the relative amount of each component can be evaluated at different depths. The measurement represents the average on the sampled zone, that usually contains several single particles with the contribution of their native-oxide coatings. The relationship between the ratio Al_{met}/Al_{ox}, the oxide thickness s and the particle average diameter d, seen by the XPS probe, is given by

$$Al_{met}/Al_{ox} = d/4s.$$

The knowledge of this ratio Al_{met}/Al_{ox} gives much information concerning the metallic-particle size and the coating-oxide thickness at the surface at different erosion times. The coating-oxide thickness was estimated by using data after a sputtering time long enough (12 min) to observe a steady surface (constant Al_{met} and Al_{ox} concentrations). This kind of estimation requires particle size much less than beam size, and coating thickness (s) much less than the average particle diameter (d). On the average, the surface is a sheet occupied by metal particles (circles of diameter d) and oxide (circle crowns of thickness s). The relative abundance of metal and oxide fraction can be related to s by considering circles with radius $d/2$ and circles with radius $d/2 + s$. The XPS spot diameter is 0.8 μm, so in the case of larger particles this estimation procedure does not work because all particle areas cannot be analysed, but for almost all samples (nanometric particles) an estimation of s (the thickness of sputtered metal particles) can be given. Table 3 shows the Al_{met}/Al_{ox} ratio and its variation with particle diameter.

Three main elements, Al, O, and N, characterize the chemical depth profile of sample Al_01a (figure 4). The relative atomic concentrations are constant in the bulk after 7 min of sputtering, suggesting a homogeneous composition with depth, typical for a system made of particles much smaller than the analysed area. The concentration values are: total—Al 64 at.%; O 32 at.%; N 2 at.%. The aluminium amount can be separated, by Al-peak decomposition, into metallic Al and oxidised Al, at different sputtering time. By decomposing the Al peak, and by

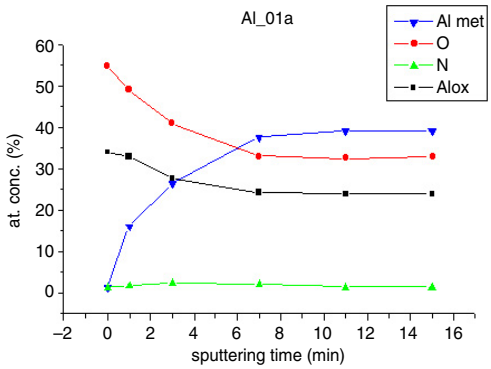

Figure 4. Chemical profiles of atomic composition obtained by XPS, for powders of series Al_01a.

Table 3. Results of atomic concentrations per unit volume, obtained by XPS (data obtained after 12 min of sputtering).

Al powder notation	Atomic%				
	O	Al	N	O/Al_{ox}	Al_{met}/Al_{ox}
Al_01a	33 (±2)	63 (±4)	1.5	1.4	1.6
Al_02a	35	62	2	1.2	1.1
Al_02b	35	61	2	1.3	1.2
Al_02c	46	51	3	2.1	1.3
Al_03a	15	85	—	0.9	3.8
Al_03d	22	76	—	1.4	3.8
Al_05	12	87	—	0.8	4.8
Al_06	12	92	—	1.3	14.3

considering the presence of a small percentage of AlN (2 at.%), the total Al splits into 38 at.% of metal-Al and 24 at.% of oxidized Al. A value close to 1.5 for the ratio O/Al_{ox} suggests that the aluminium oxide is stoichiometric Al_2O_3. Iron and molybdenum contamination have also been detected at very low concentration (<1 at.%) in the bulk. Ageing effects are shown in figure 5 for the type Al_02 powders.

XPS chemical profiles for propellants including type Al_03 powders (figure 6) do not show nitrogen content; AlN is formed only under severe conditions typical of the EEW production technique. Al_03d particles are larger: the relative amount of surface oxide in the tested volume decreases with respect to the bulk material and the metal-Al contribution is thus more apparent. The ratio O/Al_{ox} is approximately 2 (mixing oxide–hydroxide) at the external surface, but is 1 in the bulk, suggesting a substoichiometric oxide at the particle surface. No difference in the oxide stoichiometric ratio O/Al_{ox} was observed when the nominal size was changed from 0.2 to 2.5 μm.

The chemical profiles of sample Al_05 are similar to the ones of type Al_03: metal-Al is the prevailing element even at higher concentration (see table 3). Moreover, the ratio O/Al_{ox} is 2 (mixing oxide–hydroxide) at the external surface and 1 in bulk, as before. Also the chemical profiles of sample Al_06 are similar to the previous ones; again metal-Al is the prevailing element and the ratio O/Al_{ox} tends to reach 1 in bulk. In this case, a small amount (around 1 at.%) of metallic iron is detected at the surface, under the thin native oxide.

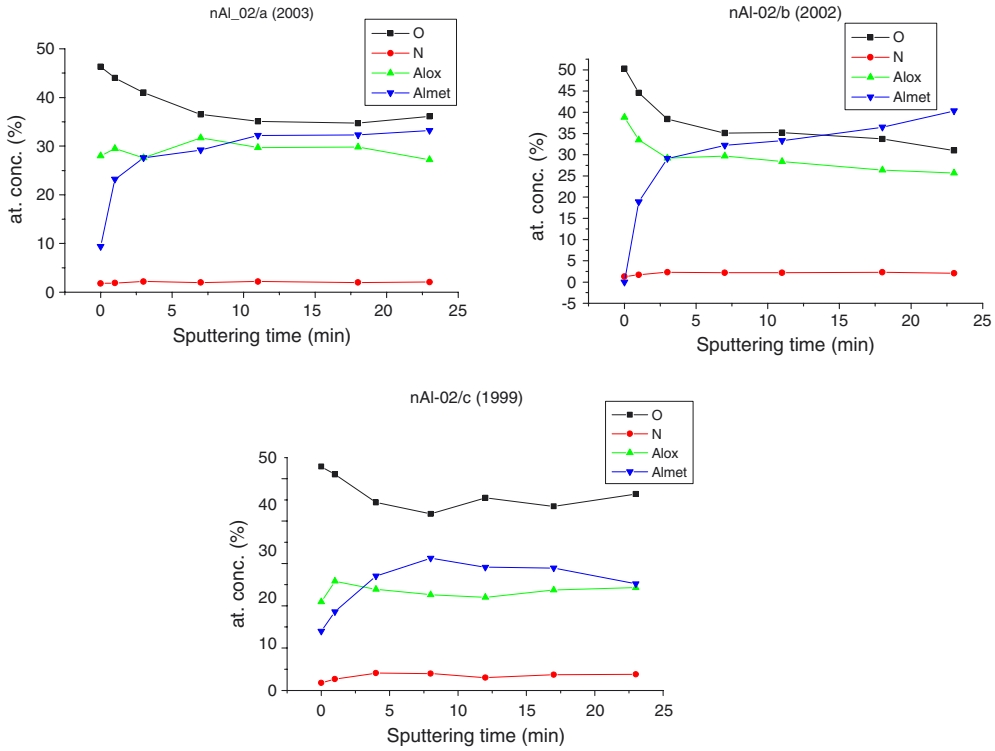

Figure 5. Chemical profiles of atomic composition obtained by XPS, for powders of type Al_02: (a) powder Al_02a; (b) powder Al_02b; (c) powder Al_02_c.

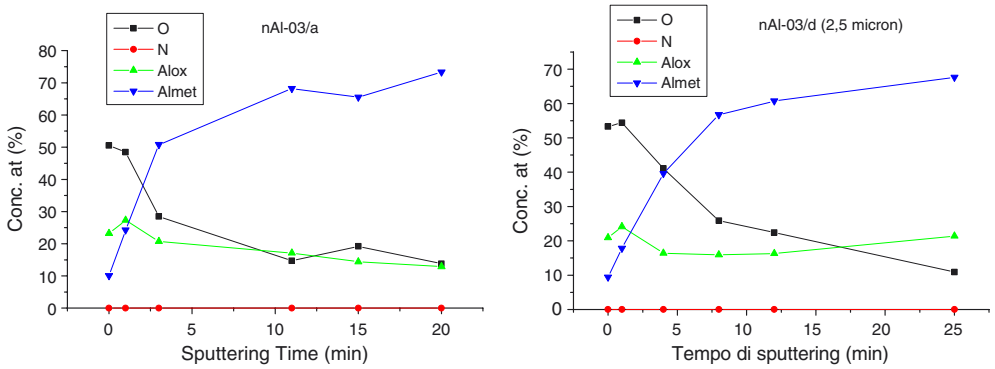

Figure 6. Chemical profiles of atomic composition obtained by XPS, for powders of type Al_03: (a) powder Al_03a; (b) powder Al_03d.

3.4. X-ray diffraction analysis (XRD)

The crystalline phases and their relative amounts, obtained by XRD, are summarized in table 4. As can be observed, all samples prepared by EEW contain two crystalline phases: the larger fraction is metallic aluminium (Al $>$ 90%), but a small fraction of aluminium nitride (AlN $<$ 10%) is also detected. In the XRD pattern no preferred orientation peaks were detected, as also confirmed by Rietveld analysis. The EEW technique implies a metal wire melting with

Table 4. Results obtained by XRD technique. Identified crystalline phases, their fraction (%) and their extension.

Al powder notation	Identified phases			
	Al		AlN	
	%	Φ (nm)	%	Φ (nm)
Al_01a	96.5	150 ± 20	3.5	20 ± 5
Al_02a	95.5	160 ± 10	4.5	35 ± 5
Al_02b	94.1	150 ± 10	5.9	32 ± 2
Al_02c	92.2	150 ± 10	7.8	34 ± 5
Al_03a	100	∞	—	—
Al_03b	100	∞	—	—
Al_03c	100	∞	—	—
Al_03d	100	98	—	—
Al_05	100	200	—	—
Al_06	100	∞	—	—

subsequent recrystallization, in N_2 atmosphere. This preparation condition is able to activate nitrogen. Moreover, the N concentration found by XPS (a few at.%) is in agreement with the AlN crystalline fraction found by XRD. The aluminium oxide which covers the metallic Al must be completely amorphous and hence is mute for XRD. In contrast, samples obtained by other techniques only contain metallic aluminium (100%) as the crystalline phase.

The crystalline domain sizes (Φ) are also determined by XRD; they represent the maximum extension of ordered regions. Amorphous material can embed the crystals and this is the reason why this length is lower than particle size.

Powder Al_01a contains two crystalline phases: metallic aluminium (Al 96.5%) and aluminium nitride (AlN 3.5%). Their average crystalline domain lengths (Φ) are 130 and 20 nm, respectively. Samples of type Al_03 present an infinite length of crystalline domains; conventionally this means they are greater than 500 nm. Samples of Al_01 and Al_02 type show domains varying from 130 to 150 nm, while Al_05 shows 200 nm.

4. Solid propellants investigated

Different propellant compositions were tested according to a reference composite formulation consisting of 68% ammonium perchlorate (AP), 17% HTPB binder, and 15% aluminium (Al). All tested compositions contain 83% mass fraction of solids (AP + Al). The size distribution of AP particles is bimodal (see tables 5 and 6) while the nature and size distribution of Al particles is monomodal or bimodal according to tables 5 and 6, but always for a total mass fraction of 15%. The binder used is the common Hydroxyl-Terminated PolyButadiene–DiOctilAdipate-IsoPhorone-DIsocyanate (HTPB–DOA-IPDI). Bimodal AP size distributions are based on a coarse/fine ratio of 4 ($c/f = 4$): coarse particles (80%) are in the range 150 ± 10 μm and fine particles (20%) in the range 75 ± 5 μm. Bimodal Al size distributions are based on a mixture of coarse (micrometric) and fine (nanometric) particles. Coarse particles are the 30 μm particles of the powder Al_05, while fine particles are in the range 0.1–0.2 μm.

All propellant formulations were designed and manufactured in small batches, at most of 100 g, in the chemical laboratory of the SPLab (Solid Propulsion Laboratory) of Politecnico di Milano.

Two different propellant series were investigated. Propellants of series I include only monomodal Al distribution (see table 5); they were prepared to assess how the burning rate

Table 5. Series I propellant formulations: bimodal AP, monomodal Al, HTPB R-20 binder.

		Al (15%)			
Propellant notation	AP size (μm)	Al powder notation	Nominal size (μm)	Binder (17%)	Propellant density (g cm^{-3})
P_06	70–80	100% Al_ 06	50	HTPB R-20	1.59
P_05	(20%)	100% Al_05	30		1.52
P_03d	140–160	100% Al_03d	2.5		1.56
P_04a	(80%)	100% Al_04a	0.2		1.69
P_01a		100% Al_01a	0.1		1.67

Table 6. Series II propellant formulations: bimodal AP-1 ($c/f = 4$), bimodal Al, HTPB R-20 binder.

		Al (15%)			
Propellant notation	AP size (μm)	Al powder notation	Nominal size (μm)	Binder (17%)	Propellant density (g cm^{-3})
P_Al_01a	70–80 (20%)	80% Al_05 20% Al_01a	30 0.1	HTPB R-20	1.61
P_Al_02a	140–160 (80%)	80% Al_05 20% Al_02a	30 0.17		1.61
P_Al_02b		80% Al_05 20% Al_02b	30 0.17		1.61
P_Al_02c		80% Al_05 20% Al_02c	30 0.17		1.53
P_Al_03a		80% Al_05 20% Al_03a	30 0.2		1.52
P_Al_03b		80% Al_05 20% Al_03b	30 0.4		1.56
P_Al_03c		80% Al_05 20% Al_03c	30 0.8		1.58
P_Al_03d		80% Al_05 20% Al_03d	30 2.5		—
P_Al_04a		80% Al_05 20% Al_04a	30 0.20		1.65
P_Al_04b		80% Al_05 20% Al_04b	30 0.28		1.64

scales with Al particle size. Propellant P_05 includes 100% of the used in propulsive applications (spheres of 30 μm diameter). Propellant P_03d includes Al_03d particles (2.5 μm nominal size); propellant P_04a includes Al_04a particles (0.2 μm nominal size and protected by a hydrocarbon coating); propellant P_01a includes Al_01a particles (0.1 μm nominal size). Propellant P_06 includes 100% of micro-Al_06, a low-cost commercial powder. All propellants of series II (see table 6) were manufactured to investigate specific effects regarding the nano-Al powders under test. A bimodal size distribution ($c/f = 4$) of AP as oxidizer and HTPB R-20 as binder were used.

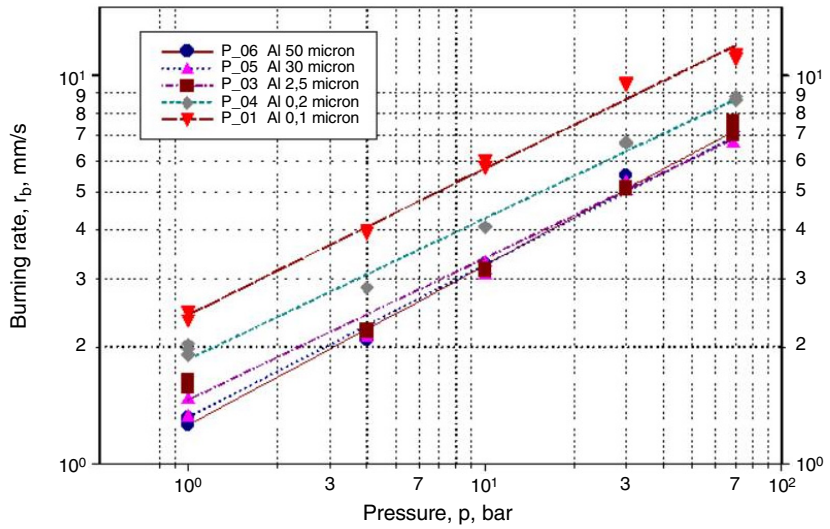

Figure 7. Measured steady burning rate for propellants of series I.

5. Steady burning rate measurements

Samples (4.5 mm × 4.5 mm × 30 mm) of the investigated propellants were burned in a nitrogen-flushed window bomb in order to measure the steady burning rate. Propellant ignition was performed by a hot Nichrome wire. Steady burning rates were measured in the range 1–70 bar, using a processing technique from high-speed video recordings. The pressure was kept constant during the whole combustion process with a feedback pressure control system.

Propellant formulations of series I, which include different nano-Al powders (Al_04a and Al_01a of table 1), have significantly higher burning rates, while propellants including Al particles in the range 2.5–50 μm (Al_03d, Al_05, and Al_06) do not exhibit appreciable difference. This trend is shown in figure 7; it can be explained by the fact that metal powders in the micrometric range (or above) burn according to a distributed mechanism, extending much beyond the gas-phase flame thickness, and thus not affecting the essentially diffusive combustion process. Ultrafine metal particles neatly increase steady burning rates because the gas-phase flame structure is now affected by the combined effects of possible earlier ignition and quick premixed burning. Experimental results in the nanometric range confirm a remarkable steady burning rate augmentation decreasing the size of the nanometric Al powder.

The standard Vieille laws for the investigated compositions are reported in tables 7 and 8. Minor changes of the burning rate pressure sensitivity show that the basic flame structure is only slightly affected.

The nano-Al_01a shows the most remarkable ballistic effects among the nano-Al powders of table 1. The steady burning rates of propellants P_Al_02a, _02b, _02c are shown in figure 8. The three powders included in the propellant composition differ only in the year of production (see table 1); the formulations using the recently produced nano-Al (_02a and _02b) showed very close results, while the formulation including nano-Al of an old production (_02c) is characterized by a systematic increase of burning rate.

These trends show that the ageing of Al particles may be important, due, in this case, to formation of $Al(OH)_3$ rather than Al_2O_3 and adsorption of gas at the particle surface. So, this result suggests the use of anti-ageing coatings for the powder passivation: it is known, for example, that commercial powders often use organic coatings.

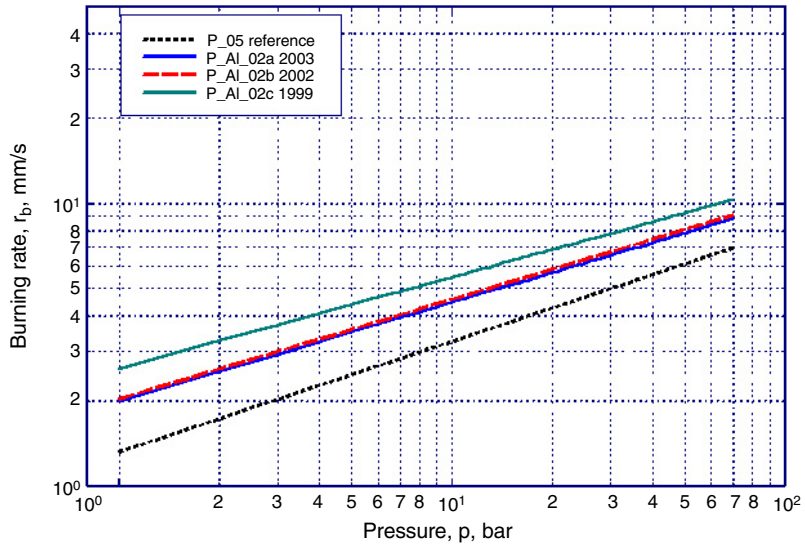

Figure 8. Steady burning rate results for propellants P_Al_02a, _02b and _02c, showing the ageing effect of the Al_02 powder.

Table 7. Steady burning rate (Vieille law) for the investigated propellants of series I.

Propellant notation	Vieille burning rate law, $r_b = ap^n$	
	a (mm s^{-1})	n ((mm s^{-1})/(bar^n))
P_01a	2.42 ± 0.07	0.38 ± 0.01
P_02b	2.00 ± 0.04	0.44 ± 0.01
P_03d	1.46 ± 0.06	0.37 ± 0.01
P_04a	1.86 ± 0.04	0.36 ± 0.01
P_05	1.32 ± 0.03	0.39 ± 0.01
P_06	1.08 ± 0.03	0.42 ± 0.01

Table 8. Steady burning rate (Vieille law) for the investigated propellants of series II.

Propellant notation	Vieille burning rate law, $r_b = ap^n$	
	a (mm s^{-1})	n ((mm s^{-1})/(bar^n))
P_Al_01a	2.61 ± 0.20	0.28 ± 0.03
P_Al_02a	1.99 ± 0.11	0.35 ± 0.02
P_Al_02b	2.04 ± 0.07	0.35 ± 0.01
P_Al_02c	2.59 ± 0.09	0.33 ± 0.01
P_Al_03a	2.82 ± 0.25	0.26 ± 0.03
P_Al_03b	2.45 ± 0.14	0.30 ± 0.02
P_Al_03c	1.82 ± 0.11	0.32 ± 0.02
P_Al_03d	NAv	NAv
P-Al_04a	2.11 ± 0.09	0.30 ± 0.02
P_Al_04b	2.93 ± 0.20	0.23 ± 0.02

Powders Al_03 were used to investigate burning rates in the range 0.2–2.5 μm. Propellants P_Al_03-a, 03b, 03c and 03d include the same powder Al_03; the only difference is the nominal

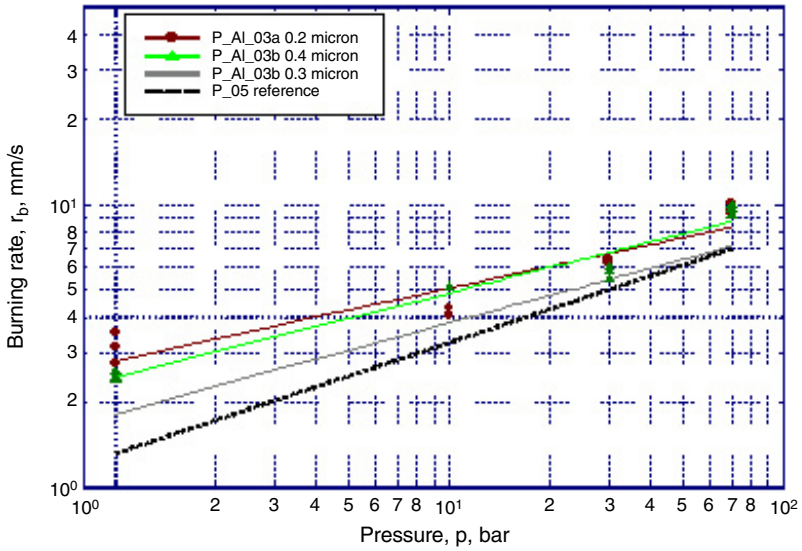

Figure 9. Similar steady burning rates for bimodal Al type 03a and 03b based propellants.

particle size, respectively 0.2, 0.4, 0.8 and 2.5 μm. Propellants P_Al_03a and Al_03b show very close burning rates; they increase in comparison with micro-Al propellants (see figure 9) while the pressure exponent decreases. SEM analyses confirm that the real dimension of both these Al powders is around 1.7 μm (average value), and this real characteristic size explains the result. The actual distribution of the Al powder Al_03c also shows a characteristic size of 1.86 μm. All powders of the type Al_03 have micrometric characteristic sizes. Also, the typical nanostructures detected in nano-Al_01a are missing in Al type 03 (see figures 1 and 2). This result shows the need for a detailed characterization of the powders because nominal specifications, in particular the powder characteristic size, can lead to incorrect interpretations.

6. The condensed combustion products analysis

Combustion of metallized solid rocket propellants results in the formation of condensed combustion products (CCPs), which have very important effects on rocket motor performance. Condensed products relate to agglomeration phenomena at the propellant burning surface. Agglomerates are systems made of aluminium and aluminium oxide, formed during the combustion process, whose size is over a defined threshold. The influence of the oxidizer particle size on the mass of the agglomerates and the effects of binder properties on agglomeration were extensively studied by Babuk [12–15]. He showed that the binder influence is determined by the content of carbon and easily gasifying elements in the binder itself. Further studies performed by Glotov *et al* [16] pointed out influences of the binder type on the agglomeration process. Opposite effects for AP-based propellants and HMX-containing propellants on agglomerates quantities and sizes were found by these authors. Coating Al particles with high-melting temperature metal films (Ni, Cu, Fe) decreases agglomeration; a similar effect can also be reached by using organic substances for coating [17].

Results concerning the technique to collect and analyse the CCPs by this group can be found in [18].

SEM techniques were used for a visual inspection of the combustion residues. SEM analysis seems to confirm, for the investigated propellants and under the operating conditions

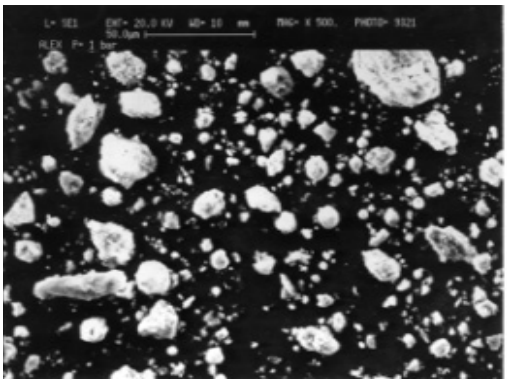

Figure 10. SEM micrograph of condensed combustion residues of P_01a propellant (magnification: 500×).

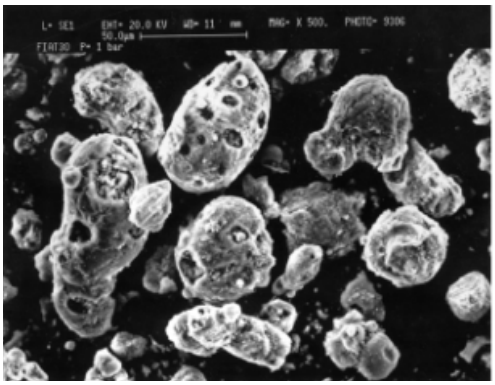

Figure 11. SEM micrograph of condensed combustion residues of P_05 propellant (magnification: 500×).

used, that agglomeration is poor for coarse Al powder, but consistent for nano-Al powder. A comparison of SEM micrographs for propellants P_01a and P_05, at a pressure of 1 bar and at the same magnification, is shown in figures 10 and 11.

XPS analysis concerns the surface of the residues, while the bulk composition is better investigated by XRD. XPS allows one to obtain interesting results: table 9 shows the total amount of atomic species in each state respectively for two representative propellants of table 5. The carbon content comes from pyrolysis processes; it is partially oxidized. Al is the total Al, mainly detected as aluminium oxide, while metal Al contained inside CCPs does not appear in the XPS analysis of the residues. Chlorine is probably chlorine from AP decomposition, entrapped in the CCPs.

XRD spectra were obtained to disclose the crystalline phases and their relative abundance; for details about the technique see [5] and [11]. The results of the x-ray powder analysis relative to the combustion products for propellants P_01a and P_05 are summarized in table 10. The condensed products contain the same inorganic phases, that is γAl_2O_3, $\delta^* Al_2O_3$, αAl_2O_3 and metallic aluminium (Al^0). The first two phases are metastable transition aluminas and the third one is the well-known corundum. The trend of aluminium content of residues suggests that the higher pressure favours the metal burning and that the burning performance of propellant P_01 is much better than P_05 ones.

Table 9. XPS analysis of the condensed combustion products of propellants P_01a and P_05.

	P_01a		P_05	
Chemical species	$p = 1$ bar at.%	$p = 30$ bar at.%	$p = 1$ bar at.%	$p = 30$ bar at.%
O 1s	49.7	45.1	46.8	45.7
Al 2s	38.2	34.0	30.2	36.2
C 1s	10.4	19.4	17.4	16.3
Cl 2p	1.4	1.1	2.4	1.3

Table 10. XRD analysis of the condensed combustion products of propellants P_01a and P_05.

Al^0 and oxides	P_01a		P_05	
	$p = 1$ bar	$p = 30$ bar	$p = 1$ bar	$p = 30$ bar
Al^0	3.6	1.5	71.9	9.8
γAl_2O_3 (%)	56.7	57.2	16.7	48.4
$\delta^* Al_2O_3$ (%)	37.4	37.7	9.0	40.0
αAl_2O_3 (%)	2.4	3.6	2.4	1.8

Although the temperatures inside the chamber are well above the value requested to get the α form ($\approx$1400 K), the transition aluminas γ and δ^* found in all the samples and their relative abundance means that these temperatures have been experienced by the residues only for very short times. Furthermore, there should be a high temperature gradient between the burning surface of the propellant and the layers below, so that the most part of the aluminium oxidized is involved in a temperature range typical of transition aluminas γ and δ^*.

7. Conclusions and future work

A detailed characterization has been performed to compare several aluminium powders, from microsize to nanosize, passivated by aluminium oxide.

The Al particle size and distribution inside the propellant are important parameters affecting the burning characteristics. The measured specific surface of Al_01a is around 15.6 $m^2\ g^{-1}$, much larger than the specific surface of Al_05 and Al_03d, both below 1 $m^2\ g^{-1}$. Al_01a, as shown by electron micrographs, is really dispersed at the nanoscopic scale as a fractal structure. The large specific surface and the fractal fine dispersion of the powder Al_01a are the key points for the higher burning rate explanation.

AP/HTPB/Al solid rocket propellants, containing Al particles of nanometric size, show faster steady burning rates compared to the corresponding compositions containing micrometric Al particles. This increase is mainly related to the intense energy released by ultra-fine particle oxidation closer to the propellant burning surface. Nano-Al particles show a very strong reactivity (equivalent to an increase of the premixed heat release contribution) due to an increased specific surface. The burning rate is essentially unaffected by particles in the micrometric range ($\geqslant 1\ \mu$m) but is strongly increased by decreasing size particles in the nanometric range (0.1–0.2 μm). All the investigated propellants showed a very similar pressure exponent.

Nano-Al increases the propellant density and the rocket specific impulse, but cost and safety problems also increase. Aggregation and agglomeration of particles is probably the most important problem to be solved when nanoparticles are used. Pre-burning aggregation

and burning agglomeration yield an increase of the apparent metal size which is detrimental for performance parameters. For this reason nano-Al particles should be coated with a protective layer to avoid pre-burning aggregation and surface oxidation and to avoid agglomeration during the burning process. Coated particles will represent the next generation of nanoparticle technology, and future work will be focused on such innovative nanoparticles.

References

[1] Mench M M, Yeh C L and Kuo K K 1998 Propellant burning rate enhancement and thermal behavior of ultra-fine aluminum powders (Alex) *Energetic Materials: Production, Processing and Characterization, Proc. 29th Int. Annual Conf. of ICT, 30-1-15 (Karlsruhe, Federal Republic of Germany)* paper No. 30

[2] Simonenko V N and Zarko V E 1999 Comparative study of the combustion behavior of fine aluminum *'Energetic Materials', Proc. 30th Int. Annual Conf. of ICT (Karlsruhe, Germany)* paper No. 21

[3] Dokhan A, Seitzman J M, Price E W and Sigman R K 2001 The effects of Al particle size on the burning rate and residual oxide in aluminized propellants *37th AIAA/ASME/SAE/ASEE Joint Propulsion Conf. and Exhibit (Salt Lake City, UT, July 2001)* AIAA Paper 2001-3581

[4] Olivani A, Galfetti L, Severini F, Colombo G, Cozzi F, Lesma F and Sgobba M 2002 Aluminum particle size influence on ignition and combustion of AP/HTPB/Al solid rocket propellants *presented at RTO Specialist's Meeting on Advances in Rocket Propellant Performance, Life and Disposal for Improved System Performance and Reduced Costs (Applied Vehicle Technology Panel (AVT), Aalborg, Denmark, Sept. 2002)*

[5] Bui D T, Atwood A I and Atienza Moore T M 2004 Effect of aluminum particle size on combustion behavior of aluminized propellants in PCP binder *Proc. 35th Int. Annual Conf. of ICT (Karlsruhe, Germany)* paper No. 27

[6] Weiser V, Eckl W, Eisenreich N, Kelzenberg S, Plitzko Y, Poller S and Roth E 2004 Burning behavior of aluminized composite propellants including nanoparticles *Novel Energetic Materials and Applications* ed L T DeLuca, L Galfetti and R A Pesce-Rodriguez (Bergamo: Grafiche GSS) paper No. 17

[7] Dokhan A, Price E W, Seitzman J M and Sigman R K 2003 The ignition of ultra-fine aluminum in AP solid propellant flames *39th AIAA/ASME/SAE/ASEE Joint Propulsion Conf. and Exhibit (Huntsville, AL, July 2003)* AIAA Paper 2003-4810

[8] Galfetti L, Severini F, DeLuca L T and Meda L 2004 Nano propellants for space propulsion *Space Propulsion 2004, 4th Int. Spacecraft Propulsion Conf. (Proceedings SP-555 of Space Propulsion 2004, ESA) (Chia Laguna (Cagliari), Italy, June 2004)*

[9] Meda L, Marra G L, Braglia R, Abis L, Gallo R, Severini F, Galfetti L and DeLuca L T 2004 A wide characterization of aluminum powders for propellants *Proc. 9-IWCP, Novel Energetic Materials and Applications (Nov. 2004)* paper No. 17

[10] Sedoi V S and Valevich V V 2001 Characterization of ultra-fine powders produced by the exploding wire method *Energetic Materials: Ignition, Combustion and Detonation. Proc. 32nd Int. Annual Conf. of ICT (Karlsruhe, Germany)* paper No. 80

[11] Vorozhtsov A B *et al* 2003 Ignition and combustion of solid and gelled propellants containing ultra-fine aluminum *Rocket Propulsion: Present and Future* ed L T DeLuca (Bergamo: Grafiche GSS) paper No. 36

[12] Babuk V A, Vassiliev V A and Malakhov M S 1999 Condensed combustion products at the burning surface of aluminized solid propellant *AIAA-JPP* **15** 783–93

[13] Babuk V A, Vassiliev V A and Sviridov V V 2000 Formation of condensed combustion products at the burning surface of solid rocket propellant *Solid Propellant Chemistry, Combustion, and Motor Interior Ballistics, AIAA Progress in Astronautics and Aeronautics* vol 185, ed V Yang, T B Brill and W Z Ren (Reston, VA: American Institute of Aeronautics and Astronautics) chapter 2.21, pp 749–76

[14] Babuk V A, Vassiliev V A and Sviridov V V 2001 Propellant formulation factors and metal agglomeration in combustion of aluminized solid rocket propellant *Combust. Sci. Technol.* 261–89

[15] Babuk V A and Vassiliev V A 2002 Model of aluminum agglomerate evolution in combustion products of solid rocket propellant *J. Propulsion Power* **18** (4)

[16] Glotov O G, Zarko V E, Karasev V V and Beckstead M W 1997 Effect of binder on the formation and evolution of condensed combustion product of metalized solid propellants *Proc. 28th Int. Annual Conf. of ICT (Karlsruhe, Germany)*

[17] Risha G A, Boyer E, Wehrman R B and Kuo K K 2002 Performance comparison of HTPB-based solid fuels containing nano-size energetic powder in a cylindrical hybrid rocket motor *38th AIAA/ASME/SAE/ASEE Joint Propulsion Conference and Exhibit (July 2002)*

[18] Galfetti L, Severini F, DeLuca L T, Marra G L, Meda L and Braglia R 2004 Ballistics and combustion residues of aluminized solid rocket propellants *Proc. 9-IWCP, Novel Energetic Materials and Applications (Nov. 2004)* paper No. 18